Mühendislik ve Yer Bilimleri Dergisi, Cilt 5, Sayı 2, 70-95 s. / Journal of Engineering and Earth Science, Volume 5, Issue 2, 70-95 p.
ISSN 2536-4561 2020 – Aralık / December http://dergipark.gov.tr/mybd

EFFECTIVE STRESS BASED ASSESSMENT OF SEISMIC STABILITY CONDITION AND PERMANENT DISPLACEMENTS OF SATURATED COHESIONLESS INFINITE SLOPES

Devrim Erdoğan[1*]

Assist. Prof. Dr. Ege University Civil Engineering Dept.;
devrim.sufa.erdogan@ege.edu.tr; devrim.ulgen@gmail.com

[*]Corresponding Author

RESEARCH ARTICLE – ENGLISH

Abstract

Seismic failure and deformation behavior of slopes is dominated by various mechanisms. Initial stress state due to static loading conditions in addition to inertial and weakening effects due to seismic excitation are among the main mechanisms. Inertial effects arise from seismic shear stresses. When they add on to initial static shear stresses, combined shear stresses may exceed available shear strength temporarily and lead to permanent displacements. Weakening effects, on the other hand, arise from straining of the soil mass giving rise to excess porewater pressure generation in cohesionless soils and cyclic degradation effects in cohesive soils which result in reduction in the available shear strength and stiffness. In the context of this paper, effective stress based seismic response analysis and Modified Newmark Method for shear strength reduction effects are used in coordination with each other in order to investigate the effect of mentioned factors on seismic stability and deformation behavior of saturated cohesionless infinite slopes.

Keywords: effective stress based analysis, seismic slope stability, inertial and weakening effects, excess porewater pressure, critical seismic acceleration coefficient, permanent displacements

Suya Doygun Kohezyonsuz Sonsuz Şevlerin Sismik Stabilite ve Deformasyon Durumlarının Efektif Gerilme Tabanlı Sayısal Analizi

Özet

Şevlerin sismik yükler altındaki göçme ve deformasyon durumları çeşitli mekanizmalar tarafından kontrol edilmektedir. Temel mekanizmalar, statik yükleme koşullarına bağlı

olan başlangıç gerilme durumu, sismik kayma gerilmelerine bağlı olan atalet etkileri ve aşırı boşluksuyu basıncı gelişimine parallel olarak meydana gelen kayma dayanımı ve rijitlik kayıplarıdır. Sismik yükleme sırasında, statik ve sismik kayma gerilmelerinin kombinasyonundan oluşan gerilme durumunun mevcut kayma dayanımını aşması durumunda kalıcı deformasyonlar meydana gelmektedir. Öte yandan, sismik yükleme sırasında meydana gelen kayma dayanımı ve rijitlik kayıpları ise, granüler zeminlerde daha çok zemin deformasyonuna bağlı olarak gelişen aşırı boşluksuyu basıncı artışlarından, kohezyonlu zeminlerde ise zeminin yumuşamasından kaynaklanmaktadır. Bu çalışma kapsamında, efektif gerilme tabanlı sismik tepki analizleri ve kayma dayanımı kayıplarını dikkate alan Modifiye Newmark yöntemi birlikte kullanılarak yukarıda sıralanan faktörlerin suya doygun kohezyonsuz sonsuz şevlerin sismik stabilite ve deformasyon durumlarında meydana gelebilecek etkiler sayısal olarak ele alınmıştır.

Anahtar kelimeler: efektif gerilme tabanlı analiz, sismik şev stabilitesi, atalet etkileri ve kayma dayanımı kaybı etkileri, aşırı boşluksuyu basıncı, kritik sismik ivme katsayısı, kalıcı yerdeğiştirmeler.

1. Introduction

Seismic failure and deformation behavior of slopes is dominated by various mechanisms. Inertial instabilities arise from seismic shear stresses caused by earthquake-induced accelerations. Pure inertial instabilities, i.e without any consideration of weakening effects are those in which there is almost no effect of reduction in shear strength and stiffness. However, limited permanent displacements are expected when combined shear stresses (seismic shear stresses+ already existing initial static shear stresses due to sloping ground) temporarily exceed available shear strength of the soil mass. Lateral permanent displacements become higher if both initial and seismic shear stresses have the same direction. Sole consideration of inertial effects without any weakening effect may be rational when there is confidence that displacement behavior during seismic excitation is not associated with reduction in shear strength (WSDOT, 2019; Brabhaharan et al., 2018; Jia, 2018).

Weakening type instabilities, on the other hand, are the instabilities which occur due to gradual reduction in shear strength and stiffness during seismic excitation. When weakening effects are in action, seismic accelerations and therefore seismic shear stresses may decrease leading to decrease in inertial effects and related deformations. Therefore, increase in the domination level of weakening effects may cause decrease in the domination level of inertial effects. However, at the same time, shear strength reduction leads to easier reach of combined shear stresses to available shear strength and temporarily exceed it. Each temporary catch up with available shear strength, causes accumulation of limited permanent displacements which may as well lead to deformation type (displacement) failures. In some of the cases, shear strength reduction may be such that, it may reduce below initial static shear stress level leading to mobilization of gravity during seismic excitation leading to flow failures and very large deformations. Flow failure may occur at excess porewater ratios smaller than 1 in sloped cases, just the reverse of level ground case where failure occurs

when excess porewater pressure ratio approaches 1, i.e approximately when full shear strength is lost.

In practice, seismic stability problem is used to be treated by pseudo-static (force based analytical method) and Newmark methods (displacement based analytical method). However, these methods in their traditional forms are usually suitable for analyzing inertial type instabilities without any consideration of shear strength reduction (weakening) effects. Considerable amount of research has been conducted in literature in order to include weakening effects in the traditional Newmark Sliding Block model (Biondi et al., 2000; Biondi et al. 2001; Biondi et al., 2002; Biondi et al., 2004; Biondi and Maugeri, 2006; Biondi et al., 2007a,b; Biondi et al., 2008; Bandini et al., 2015; Filippo and Cascone, 2019; Ingegneri et al., 2019; Jafarian and Lashgari, 2017). In the context of this paper, parametric analysis has been conducted in order to evaluate the effect of inertial and weakening type instabilities on seismic stability condition and permanent lateral displacements of infinite saturated cohesionless slopes. One-dimensional effective stress based seismic response analysis of loose, medium dense and dense infinite saturated cohesionless slopes of 40 m. height have been performed with varying slope angles of 2°, 5°, 10°, 15° and 20°. Newmark method modified for shear strength reduction effects (Biondi et al., 2002) has been used for the evaluation of critical seismic acceleration coefficients and threshold excess porewater pressure ratios for triggering of flow failure and permanent displacements, respectively. Afterwards, validity and effectiveness of these thresholds are discussed by comparing them with the results of effective stress based seismic response analysis. In addition, relationship between permanent lateral displacements and the degraded critical seismic acceleration coefficients has been investigated.

2. Newmark Method Modified for Weakening Effects (Procedure developed by Biondi et al., 2002; Biondi and Maugeri, 2006)

Traditional form of Newmark method which is widely used in the evaluation of permanent slope displacements is based on critical seismic acceleration coefficients (representing inertial effects) without any consideration of shear strength reduction. In order to fulfill this lack, effective stress based modification has been incorporated by Biondi et al. (2002) and Biondi and Maugeri (2006) into traditional Newmark method for shear strength reduction effects. In the following paragraphs, brief overview of this modification for infinite saturated cohesionless slopes has been presented through formulations (1) – (9). These formulations depend on the infinite slope scheme in Figure 1 by Biondi et al. (2002). In these formulations, seismic excitation is taken as parallel to the infinite slope which is represented by $\omega = -\beta$. Details of these formulations can be found in the related literature (Biondi et al., 2000; Biondi et al., 2001; Biondi et al., 2002; Biondi et al., 2004; Biondi and Maugeri, 2006; Biondi et al., 2007a, b; Biondi et al., 2008; Bandini et al., 2015; Filippo and Cascone, 2019; Ingegneri et al., 2019).

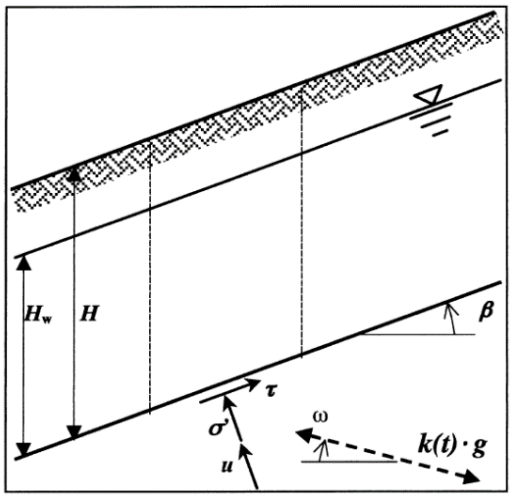

Figure 1. Infinite slope scheme (from Biondi et al., 2002).

Static Factor of Safety (Biondi et al., 2002):

$$FS_{static} = \frac{\tau_{f0}}{\tau_0} = \frac{\cos\beta(1-r_u)tan\emptyset\prime}{sin\beta} \qquad (1)$$

$$r_u = \frac{H_w}{H}\frac{\gamma_w}{\gamma}$$

Here; r_u: static pore pressure ratio, β: slope angle, ϕ': internal friction angle

Pseudo-Static Factor of Safety:

Relation (2) represents pseudo–static factor of safety in which inertial effects are represented by a constant seismic acceleration coefficient (*k*) although *k* is time varying in nature. In addition, degradation of shear strength is not taken into account in (2). Therefore, *k* in (2) is the non-degraded seismic acceleration coefficient. It represents inertial effects due to seismic accelerations without any consideration of shear strength reduction (weakening) effects.

$$FS_{pseudo-static} = \frac{\tau_{f0}}{\tau_0} = \frac{\cos\beta(1-r_u)tan\emptyset\prime}{sin\beta+k} \qquad (2)$$

Seismic Factor of Safety:

Relation (3) represents seismic factor of safety in which inertial effects are represented by time varying seismic acceleration coefficients *k(t)*. Shear strength reduction and the corresponding degradation in seismic acceleration coefficients are still not taken into consideration in Relation (3). On the other hand, in Relation (4), shear strength reduction is introduced through seismically induced excess porewater pressure ratios $r_u^*(t)$ which serve to degrade shear strength gradually during seismic excitation. Degraded shear strength in turn leads to degradation in inertial effect resulting in degraded seismic acceleration coefficient $k_u^*(t)$. Seismically induced excess porewater pressure ratios $r_u^*(t)$ could be evaluated through simple excess porewater pressure generation models (Biondi et al., 2000; Biondi et al., 2001; Biondi et al., 2002; Biondi and Maugeri, 2006; Biondi et al., 2007a, b).

$$FS_{seismic}(t) = \frac{\tau_{f0}}{\tau_0} = \frac{\cos\beta(1-r_u)tan\emptyset\prime}{sin\beta+k(t)} \quad (3)$$

$$FS_{seismic}(t) = \frac{\tau_{f0}}{\tau_0}$$

$$= \frac{\cos\beta(1-r_u)tan\emptyset'}{sin\beta + k^*(t)}\left(1-r_u^*(t)\right)$$

$$= \frac{\cos\beta(1-r_u)tan\emptyset\prime}{sin\beta\left(1+\frac{k^*(t)}{sin\beta}\right)}\left(1-r_u^*(t)\right)$$

$$= \frac{FS_{static}}{\left(1+\frac{k^*(t)}{sin\beta}\right)}\left(1-r_u^*(t)\right) \quad (4)$$

<u>*Degradation of Critical Seismic Acceleration Coefficient:*</u>

During seismic excitation, $FS_{seismic}(t)=1$ condition is imposed when shear strength along sliding surface is fully mobilized. Seismic acceleration coefficient corresponding to $FS_{seismic}(t)=1$ is the critical seismic acceleration coefficient. Permanent displacements occur when seismic acceleration coefficients attain higher values than the corresponding critical seismic acceleration coefficient value.

Non-degraded case: Pseudo-static (2) and non–degraded time varying cases (3) produce the same critical seismic acceleration value (k_c^0) which is constant during seismic excitation since no shear strength reduction is taken into consideration. If $k(t)$ attains higher values than the corresponding k_c^o ($k(t) > k_c^0$) then permanent displacements are expected to occur since in this case $FS_{seismic}(t)<1$.

$$FS_{pseudo-static} = \frac{\cos\beta(1-r_u)tan\emptyset\prime}{sin\beta+k_c^0} = 1$$

$$FS_{seismic}(t) = \frac{\cos\beta(1-r_u)tan\emptyset\prime}{sin\beta+k_c^0} = 1$$

$$k_c^0 = \cos\beta(1-r_u)\,tan\emptyset' - sin\beta$$

$$= [FS_{static} - 1]sin\beta \quad (5)$$

Degraded case: When shear strength degradation is taken into account, degraded value of critical seismic acceleration coefficient ($k_c^*(t)$) corresponding to each excess porewater pressure ratio, $r_u^*(t)$ should be evaluated (Equ. 6). If $k^*(t)$ attains higher values than the corresponding $k_c^*(t)$ $\left(k^*(t) > k_c^*(t)\right)$ then permanent deformations are likely to accumulate since this $k^*(t)$ value will make $FS_{seismic}(t)<1$. (Biondi et al., 2002).

$$FS_{seismic}(t) = \frac{\cos\beta(1-r_u)tan\emptyset\prime}{sin\beta+k_c^*(t)}\left(1-r_u^*(t)\right) = 1$$

$$k_c^*(t) = \cos\beta(1-r_u)\,tan\emptyset'[(1-r_u^*(t)] - sin\beta = [FS_{static}[(1-r_u^*(t)] - 1]sin\beta \quad (6)$$

During seismic excitation, critical seismic acceleration coefficient degrades from k_c^0 to $k_{c,min}^*$ (7) due to shear strength reduction. At the beginning of seismic loading ($t=0$ sn), seismic excess porewater pressure ratio $r_u^*(0) = 0$ and critical seismic acceleration coefficient attains the value $k_c^*(0) = k_c^0$ whether shear strength

reduction is taken into account or not. When seismic excess porewater pressure ratio $r_u^*(t)$ attains its maximum value, $r_{u,max}^*$, then critical seismic acceleration coefficient $k_c^*(t)$ attains its minimum value, $k_{c,min}^*$. Typical variation of critical seismic acceleration coefficient with respect static factor of safety for non-degraded and degraded cases are shown in Figure 2 (a) and (b) respectively.

$$FS_{seismic}(t) = \frac{\cos\beta(1-r_u)tan\emptyset'}{sin\beta+k_{c,min}^*}\left(1 - r_{u,max}^*\right) = 1$$

$$k_{c,min}^* = \cos\beta(1-r_u)\,tan\emptyset'\left(1 - r_{u,max}^*\right) - sin\beta = \left[FS_{static}\left[\left(1 - r_{u,max}^*\right] - 1\right]sin\beta \quad (7)$$

Threshold Values of , $r_{u,}^*(t)$ and $k_{c,}^*(t)$ to Identify Seismic Stability Condition of the Slope

There exist some threshold values of excess porewater pressure ratio which enable evaluation of seismic stability condition of the slope under the selected ground motion. Threshold $r_{u,f}^*$ indicates triggering of flow failure and threshold $r_{u,d}^*$ indicates triggering of permanent displacements. Typical seismic stability charts based on variation of $r_{u,f}^*$ and $r_{u,d}^*$ with respect to static factor of safety are given in Figures 3. Figure 3 (a) shows the regions where flow and deformation failures are expected and Figure 3 (b) indicates the expected dominating effects in these regions.

Threshold to trigger flow failure, $r_{u,f}^*$: During seismic excitation, shear strength may reduce to such a level that it catches up with the static shear stress level which is present before initiation of seismic excitation. In such cases, gravity works and flow failure occurs leading to large deformations. In this case, excess porewater pressure generation is not so high to cause mean effective stresses to vanish completely and shear strength is not fully lost. On the other hand, in cases where excess porewater pressure generation is so high, flow failure occurs due to liquefaction in which mean effective stresses approach zero and shear strength is lost gradually during seismic excitation

In both cases, critical seismic acceleration coefficient attains the value of zero when flow occurs. Imposing $FS_{seismic}(t)=1$, and $k_c^*(t) = 0$ in Equation (6), $r_{u,f}^*$ is evaluated as follows:

$$FS(t)_{seismic} = 1$$
$$= \frac{\cos\beta(1-r_u)tan\emptyset'}{sin\beta}\left(1 - r_{u,f}^*\right)$$
$$= FS_{static}\left(1 - r_{u,f}^*\right)$$
$$r_{u,f}^* = 1 - \frac{1}{FS_{static}} \quad (8)$$

Or directly from;

$$k_c^*(t) = 0 = \cos\beta(1-r_u)\,tan\emptyset'(1 - r_{u,f}^*) - sin\beta = \left[FS_{static}\left[\left(1 - r_{u,f}^*\right) - 1\right]sin\beta$$
$$r_{u,f}^* = 1 - \frac{1}{FS_{static}}$$

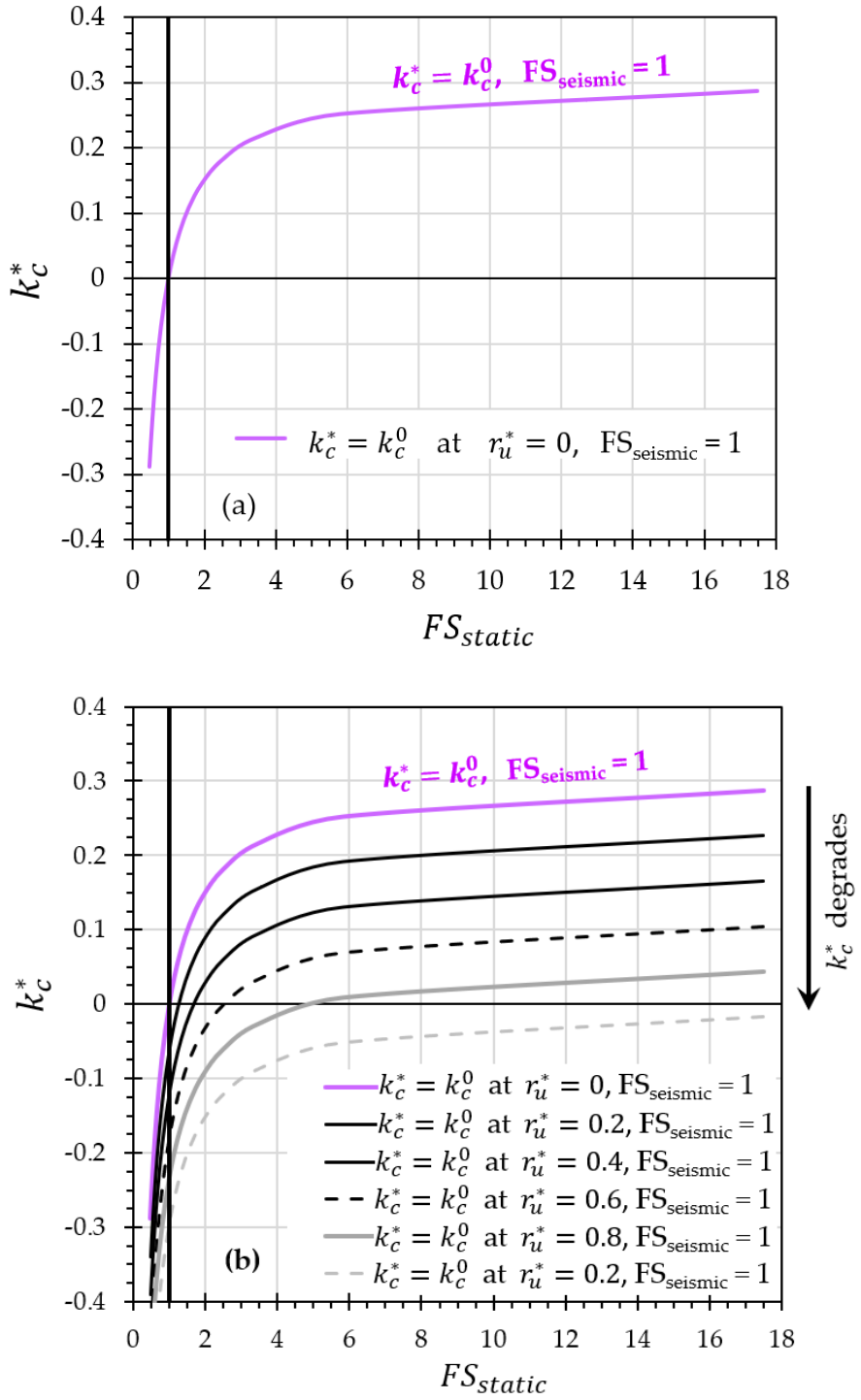

Figure 2. Typical variation of critical seismic acceleration coefficient with respect to static factor of safety for (a) non–degraded case (b) degraded case

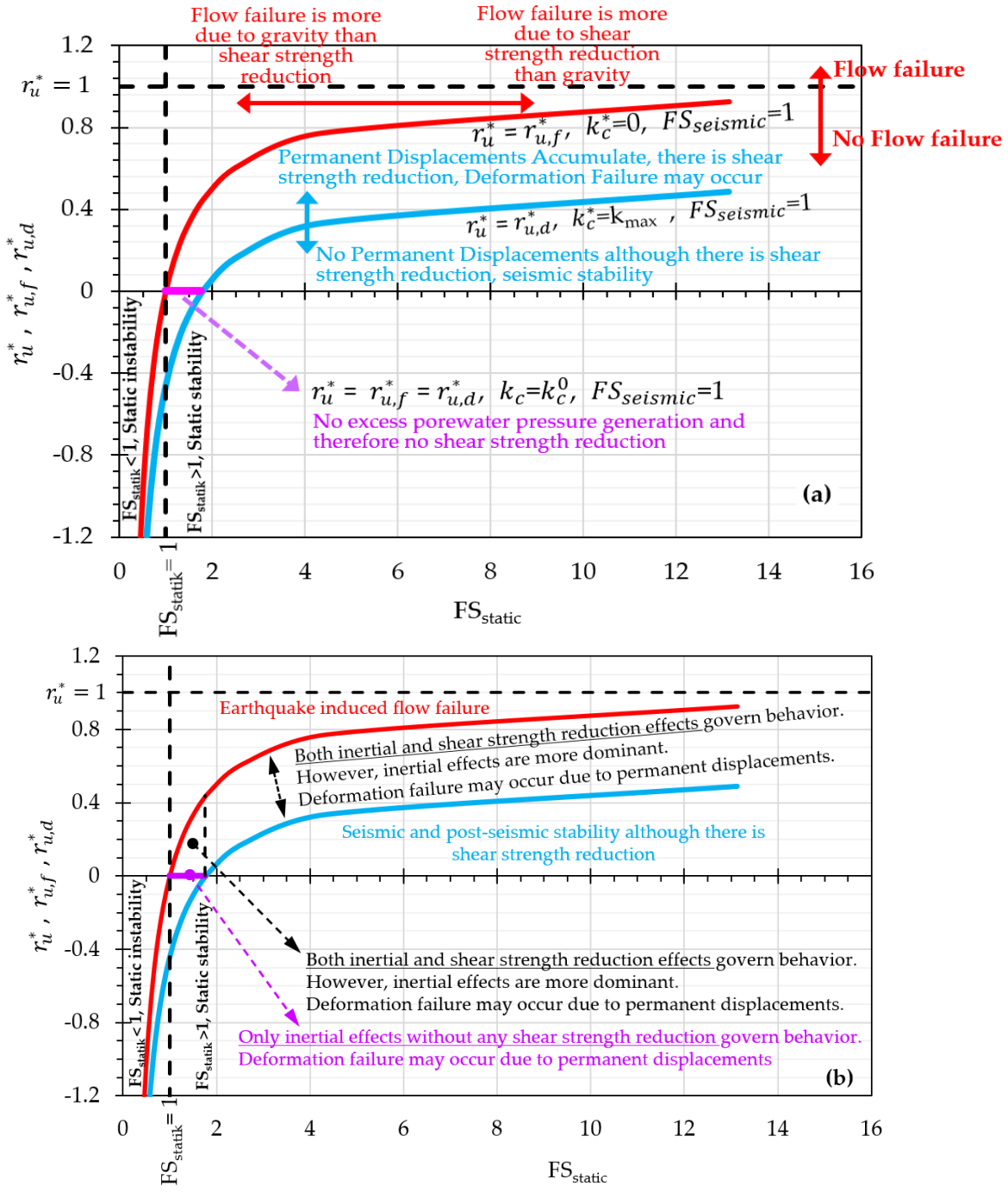

Figure 3. a) Typical chart showing seismic slope stability condition b) The same chart showing regions dominated by inertial effects only, by weakening effects only or by both inertial and weakening effects (Original figures and concepts can be found in Biondi et al., 2002 and Biondi and Maugeri, 2006).

It was stated in Biondi et al. (2000) that " $r^*_{u,f}$ *is a characteristic of the slope and it does not depend on seismic accelerations and earthquake-induced effective stress state"*

Threshold to trigger permanent displacements $r^*_{u,d}$: Imposing $FS_{seismic}(t)=1$, and $k^*_c(t) = k_{max}$ in Equation (6), $r^*_{u,d}$ is evaluated as in (Equ. 9). $r^*_{u,d}$ represents the threshold excess porewater pressure ratio for triggering of permanent slope displacements. This means;

For $r^*_u < r^*_{u,d}$ permanent displacements do not develop although there is shear strength reduction.

For $r^*_u \geq r^*_{u,d}$ permanent displacements absolutely develop.

It is also clear that $r^*_{u,d}$ depends on seismic accelerations occurring in the sliding mass (k_{max}) in addition to static stability condition (FS_{static}) of the slope.

$$FS(t)_{seismic} = 1 = \frac{\cos\beta(1-r_u)tan\emptyset'}{sin\beta+k_{max}}(1-r^*_{u,d})$$

Or directly from;

$$k^*_c(t) = k_{max} = \cos\beta(1-r_u)\,tan\emptyset'(1-r^*_{u,d}) - sin\beta$$

$$r^*_{u,d} = 1 - \frac{1}{FS_{static}} - \frac{k_{max}}{sin\beta.FS_{static}} \qquad (9)$$

3. Numerical Model for Effective Stress Based Seismic Response Analysis

Finite Element Model of the Problem

Parametric analysis are conducted in OpenSeesPL which is a graphical user interface for the finite element analysis of 3D soil and soil-structure interaction problems under seismic loading conditions. All the computations are performed in Opensees open–code environment. The power of this environment comes from the soil models inside which are capable of simulating most important aspects of nonlinear soil behaviour during seismic loading. In addition, numerical procedures for the solution of nonlinear dynamic problems are extensive.

Finite element model of the problem is a 3D soil column which is constituted by three dimensional 8 noded brick u–p elements. These elements are 1 m. in both longitudinal and transversal directions and their height is arranged such that the layer can propagate frequencies of minimum 25 Hz. according to ($f_{max}=V_s/4H$). Depth of the soil medium is 40 m. Loose, medium dense and dense states are considered with varying slope angles for which static factor of safeties (FS_{static}) are presented in Table 2. In addition, groundwater table is at the ground surface. Pressure-Dependent Multi–Yield Surface Plasticity model is used to represent the soil medium. Model parameters for loose, medium dense and dense soil profiles are given in Table 1. Seismic excitation is prescribed along the mesh base as total dynamic lateral motion. Bottom of the soil profile is considered as rigid. The lateral mesh

borders undergo shear–beam type motions (equal motion of lateral boundaries is enforced, tied degrees of freedom boundary condition) in order to represent one dimensional (1D) seismic site response behavior. The slope in this example is simulated as a static shear stress generated by applying gravity with components in the the y – and z–directions. Lateral Acceleration (g) – time (s) history of input seismic excitation is given in Figure 4.

Pressure Dependent Multi-Yield Surface Plasticity Model (PDMY)

PDMY is an effective stress based plasticity model developed for the representation of granular soil behavior under dynamic loading conditions (Parra, 1996; Elgamal et al., 1998; Elgamal et al., 2003; Elgamal, 2014). Advantage of effective stress based models is that variation in shear strength and rigidity due to variation in mean effective stress level can be traced with respect to time. Variation in excess porewater pressures is among the major causes leading to variation in mean effective stress level. PDMY model is based on multi–surface yield concept in which yield surfaces are conical. Outermost yield surface defines the failure surface and middle surfaces represent the hardening region. The size of the failure surface is represented by friction angle. Backbone stress–strain curve is derived from yield surfaces and G/G_{max} curve is obtained from backbone stress–strain curve. Backbone curve and hence G/G_{max} curve are pressure-dependent. Flow rule defines deviatoric and volumetric plastic strain behavior. Deviatoric plastic strain behavior follows associative flow rule in which yield surface is used for its representation. Volumetric plastic strain behavior follows nonassociative flow rule which is not defined by yield surface, instead, defined by phase transformation concept (Opensees calibration manual)

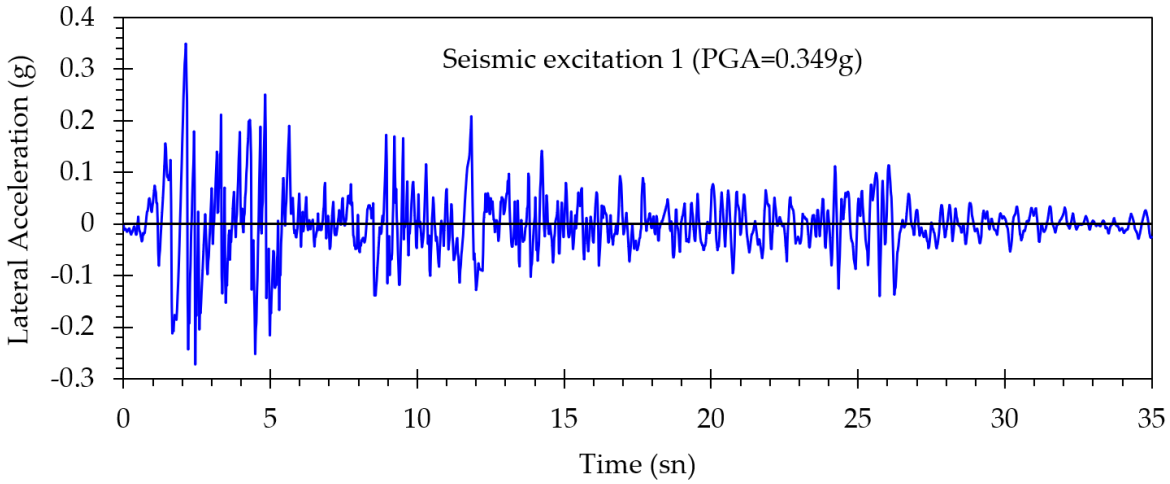

Figure 4. Horizontal acceleration time histories.

Table 1. PDMY model parameters

	Loose	Medium Dense	Dense		Loose	Medium Dense	Dense
SOIL ELASTIC PROPERTIES				DILATANCY / LIQUEFACTION PROPERTIES			
Saturated mass density, ρ (kg/m^3)	1800	1900	2000	Phase transformation angle, ϕ_P **(°)**	27	27	27
Reference shear modulus, p'_{ref} (kPa)	100	100	100	Contraction parameter, c_1	0.12	0.06	0.04
Confinement Dependent Coefficient, n	0.5	0.5	0.5	Dilation parameter, d_1	0	0.3	0.5
Reference shear modulus, $G_{max,ref}$ (kPa)	53508	75000	100000	Dilation parameter, d_2	0	2	3
Reference bulk modulus, $B_{max,ref}$ (kPa)	139477	200000	300000	Liquefaction parameter, Liq 1	10	10	5
SOIL NONLINEAR PROPERTIES				Liquefaction parameter, Liq 2	0.02	0.01	0.003
Cohesion, c (kPa)	0	0	0	Liquefaction parameter, Liq 3	1	1	1
Friction angle, ϕ (°)	27	33	38				
P, γ_{max} (%)	10	10	10				
Number of Yield surfaces, NYS	30	30	30				

Table 2. Static factor of safeties for various slope angle values of loose, medium dense and dense infinite slopes (Evaluated by Relation (1))

Slope angle (°)	Loose ϕ=27°, r_u=0.55	Medium dense ϕ=33°, r_u=0.53	Dense ϕ=38°, r_u=0.50
	FS_{static}	FS_{static}	FS_{static}
2	6.5	8.8	11.2
5	2.6	3.5	4.5
10	1.3	1.7	2.2
15	-	1.1	1.46
20	-	-	1.07

4. Results and Discussion

Threshold for Triggering of Flow Failure ($r^*_{u,f}$)

$r^*_{u,f}$ thresholds are evaluated by using Relation (8) for a large range of slope angles up to internal friction angle for each of loose, medium dense and dense soil profiles This range is 1°–27° for the loose state, 1°–33° for the medium dense state and 1°-38° for the dense state. Each threshold value is then plotted with respect to the corresponding static factor of safety (Figure 5). Static factor of safeties are evaluated by relation (1). Note that $r^*_{u,f}$ curves for each of loose, medium dense and dense states fall approximately on the same curve. Black markers in Figure 5 represent cases on which effective stress based seismic response analysis is conducted. Table 1 shows $r^*_{u,f}$ thresholds for the analysed cases with the corresponding slope angles and FS_{static} values.

Negative $r^*_{u,f}$ values $(r^*_{u,f} < 0)$ represent slope angles resulting in $FS_{static}<1$ while positive values $(r^*_{u,f} \geq 0)$ represent cases with $FS_{static}>1$. For the loose state, slope angle > 12°, for the medium dense state slope angle > 16° and for the dense state slope angle > 22°, represent cases with ($r^*_{u,f} < 1$ and $FS_{static} < 1$).

It can be inferred from Figure 5 that, if $r^*_u > r^*_{u,f}$ during seismic excitation, flow failure is strongly expected in that part of the slope. Excess porewater pressure generation necessary for triggering flow type of failure strongly depends on the corresponding FS_{static} value of the slope. It is clear that flow failure may occur in a wide range of FS_{static}, however, it is the cause of the flow failure which differs during this wide range. (Table 4).

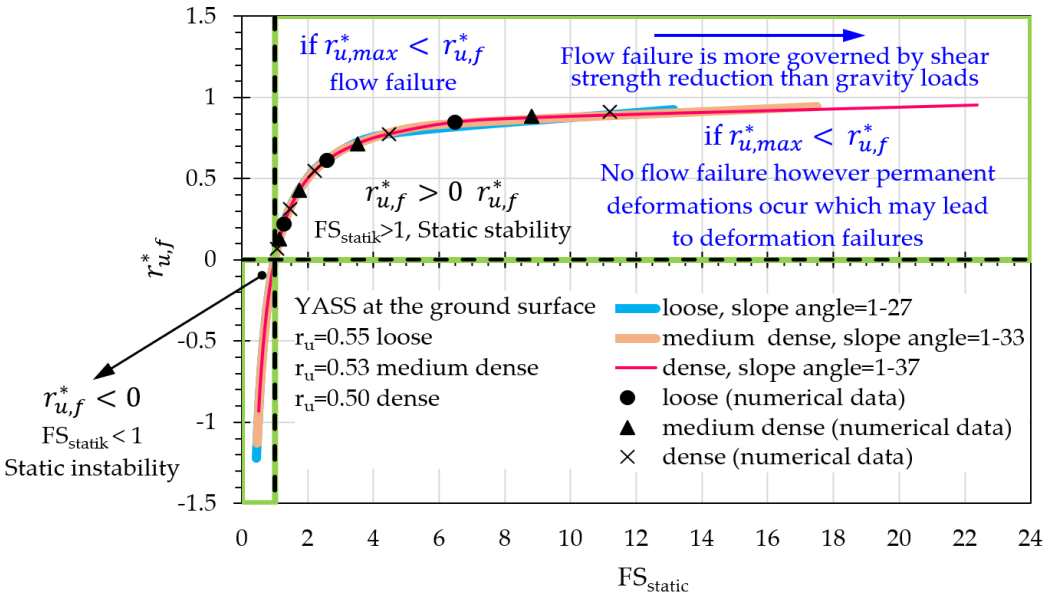

Figure 5. Variation of $r^*_{u,f}$ with FS_{static} for loose, medium dense and dense states.

Table 3. $r^*_{u,f}$ values for the cases analysed with effective stress based seismic response analysis.

Slope angle β (°)	Loose ϕ=27°, r_u=0.55		Medium dense ϕ=33°, r_u=0.53		Dense ϕ=38°, r_u=0.50	
	FS_{static}	$r^*_{u,f}$	FS_{static}	$r^*_{u,f}$	FS_{static}	$r^*_{u,f}$
2	6.5	0.85	8.8	0.89	11.2	0.91
5	2.6	0.61	3.5	0.72	4.5	0.78
10	1.3	0.22	1.7	0.43	2.2	0.55
15	-	-	1.1	0.13	1.46	0.31
20	-	-	-	-	1.07	0.07

Table 4. Interpretation of $r^*_{u,f}$ thresholds with respect to FS_{static}.

As FS_{static} increases	**As FS_{static} decreases**
Slope angles are lower	Slope angles are higher
Density state governs more	Density state seems to loose its dominance
Flow failure is triggered at higher $r^*_{u,f}$	Flow failure is triggered at lower $r^*_{u,f}$
Flow failure is dominated by shear strength reduction due to excess porewater pressure generation more than gravity due to initial static shear stress level.	Flow failure is dominated by gravity due to initial static shear stress level more than shear strength reduction due to excess porewater pressure generation.

Threshold for Triggering of Permanent Displacements $(r^*_{u,d})$:

$r^*_{u,d}$ thresholds are evaluated (Eq. 9) for the same range of slope angles as in $r^*_{u,f}$. In order to evaluate $r^*_{u,d}$ thresholds, maximum value of seismic acceleration coefficient ($k_{max} = a_{max}/g$) needs to be evaluated for the soil profile. It is clear from effective stress based seismic response analysis that the soil profile is highly flexible and deformable. Therefore, it would be unreasonable to evaluate a single k_{max} value for the whole soil profile. Instead, it would be more appropriate to observe its variation along depth and evaluate a range for it. Figure 6 (a), (b) and (c) show the variation of horizontal acceleration values along depth for each of loose, medium dense and dense states, respectively, obtained from effective stress based seismic response analysis. Depending upon these figures, the soil profiles behave highly nonlinear during seismic excitation. Appropriate range for k_{max} values is selected as k_{max}=*0.4 – 0.1*.

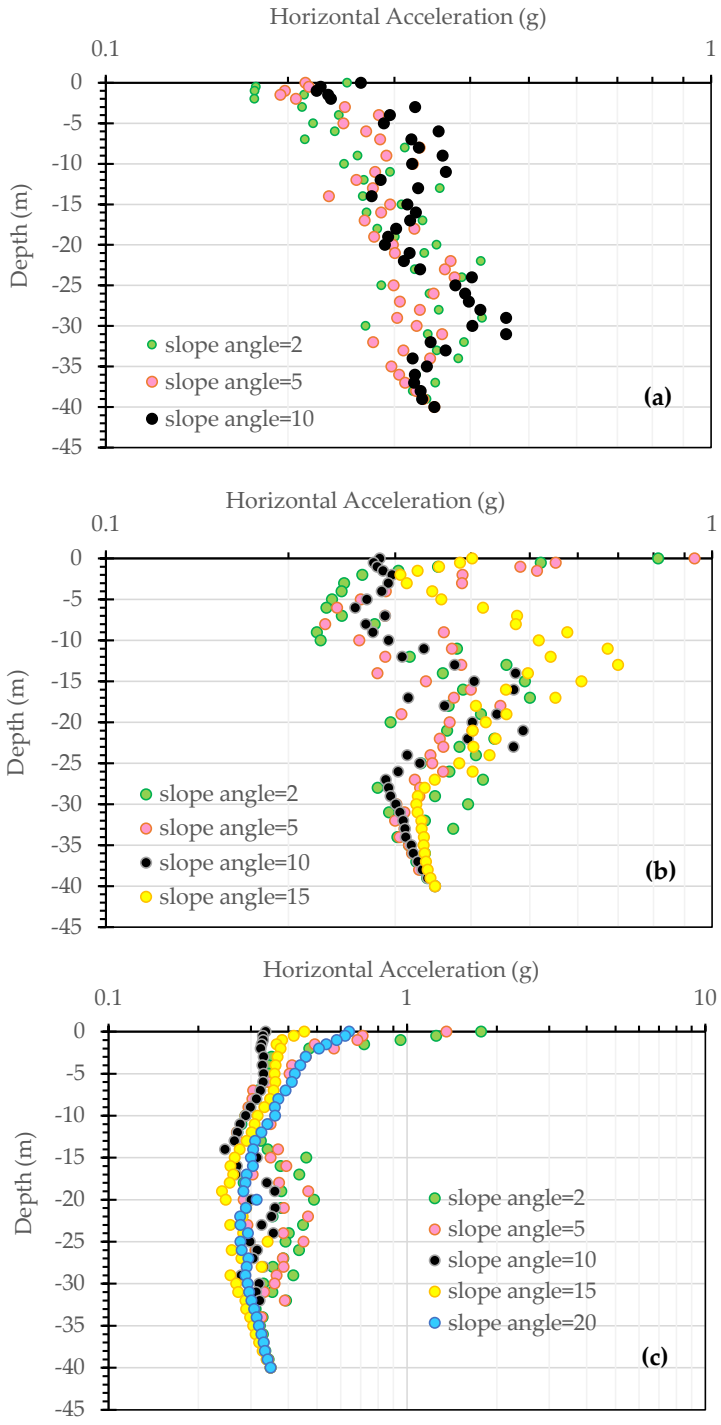

Figure 6. Variation of horizontal accelerations with depth for various slope angles of (a) loose, (b) medium dense and (c) dense states (Evaluated by effective stress based finite element analysis).

Figures 7 (a), (b), (c) and (d) show $r^*_{u,d}$ thresholds evaluated for various seismic acceleration coefficients of k_{max}=0.35 (peak acceleration coefficient of input motion), 0.2, 0.1 and 0.01, respectively. Each threshold value is then plotted with respect to the corresponding FS_{static} for

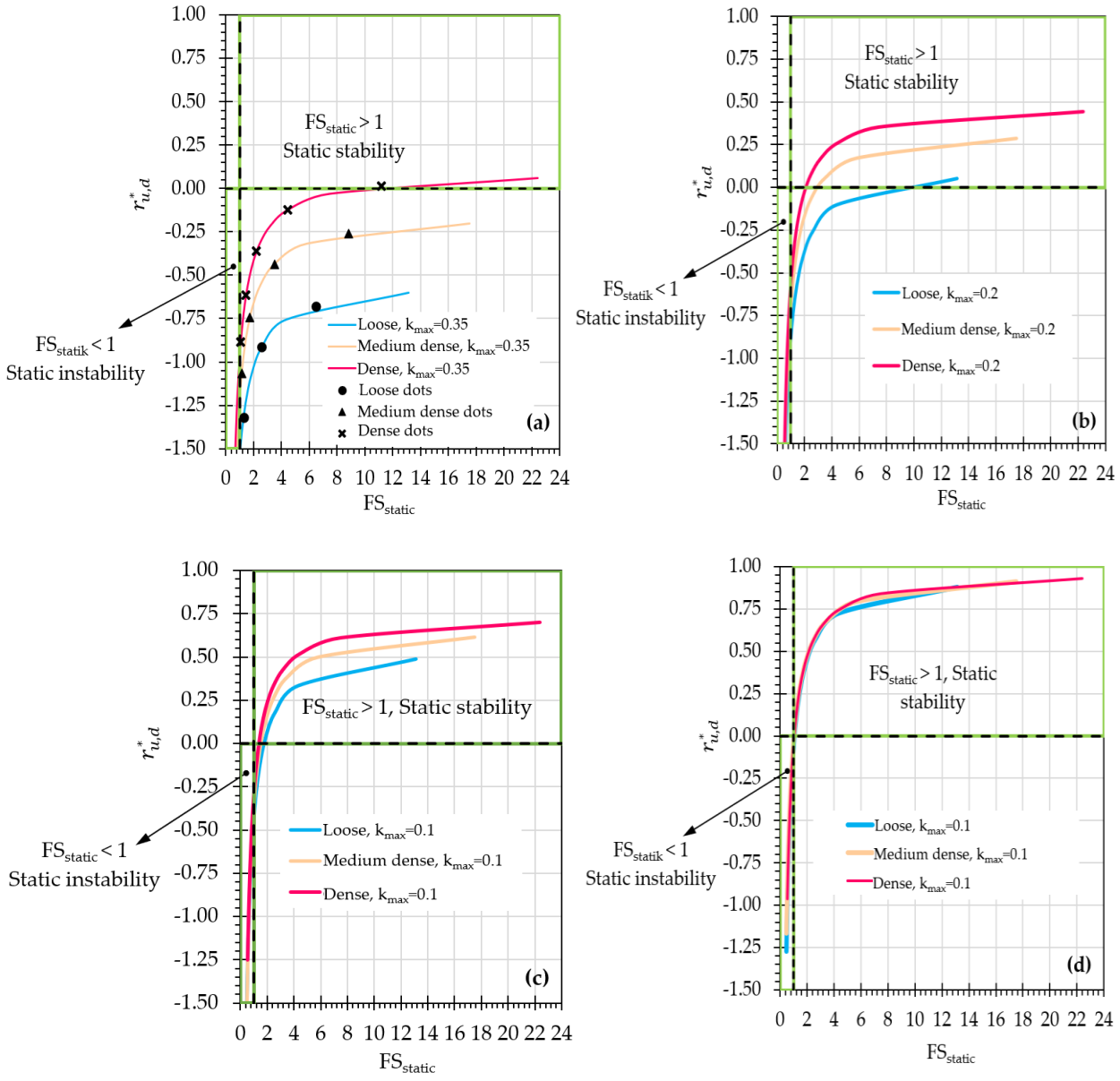

Figure 7. Variation of $r^*_{u,d}$ with FS_{static} for loose, medium dense and dense states a) k_{max}=0.35 b) k_{max}=0.2 c) k_{max}=0.1 d) k_{max}=0.01.

each of loose, medium dense and dense soil profiles. Black markers in Figure 7 (a) represent $r^*_{u,d}$ values for the cases considered in the effective stress based seismic response analysis.

$r^*_{u,d}$ curve signifies a threshold for permanent displacements where excess porewater pressure ratios below it ($r^*_u < r^*_{u,d}$) are not expected to produce any permanent lateral displacements although there is shear strength reduction. Unlike $r^*_{u,f}$ thresholds, the $r^*_{u,d}$ thresholds are not unique, i.e they vary depending upon applied seismic excitation. According to Figure 7, $r^*_{u,d}$ thresholds tend to increase w hen seismic accelerations decrease meaning that lateral permanent displacements are not expected despite shear strength reduction due to high levels of seismic excess porewater pressure generation. In addition, $r^*_{u,d}$ value is less affected by relative density when seismic accelerations get lower which is very significant from Figure 3 (d).

Charts for Seismic Stability Condition of the Slopes:

$r^*_{u,f}$ and $r^*_{u,d}$ threshold curves corresponding to each density state have been superposed (Figure 8 a, b and c) and maximum excess porewater pressure ratios ($r^*_{u,max}$) along depth of each profile obtained from effective stress based seismic response analysis have been plotted on the corresponding charts (blue bars). Comparison of $r^*_{u,max}$ with the corresponding $r^*_{u,f}$ and $r^*_{u,d}$ threshold enables the prediction of the type of response and instability (inertial or weakening or inertial + weakening) expected

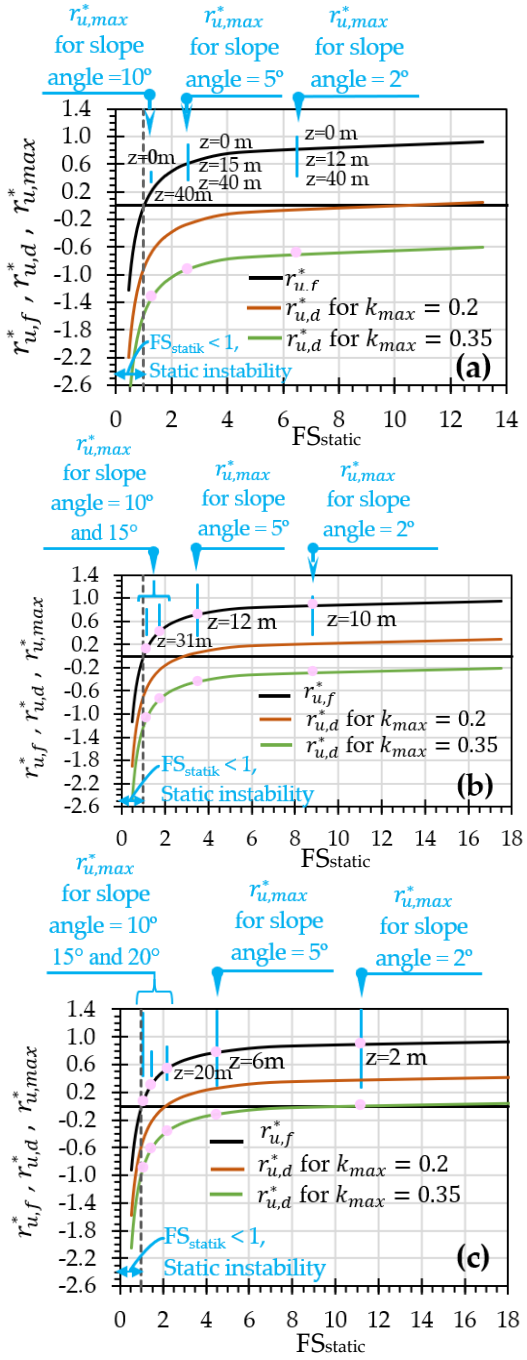

Figure 8. Variation of $r^*_{u,f}$, $r^*_{u,d}$ and $r^*_{u,max}$ with FS_{static} for (a) loose, (b) medium dense and (c) dense soil profile

to occur in the sloped profile due to applied seismic excitation. Under the applied seismic excitation, it seems that permanent lateral displacements are expected all along depth of each profile since $r^*_{u,max} > r^*_{u,d}$. Some of these permanent displacements are due to flow failure. According to Figure 8, all the profiles exhibit flow type of failure to some depth from the ground surface which can be designated by $r^*_{u,f}$. However, this flow failure occurs mostly due to shear strength reduction effects at lower slope angles (higher FS_{static}), but, at higher slope angles (lower FS_{static}), gravity works which is very distinct from excess porewater pressure ratios and corresponding lateral displacements given in Figure 9 with respect to depth.

This aspect of seismic slope behavior can be better traced from time histories of excess porewater pressure ratios, shear strength variation, critical seismic acceleration coefficients and resulting lateral displacements. In this context, Figure 10 and 11 exhibit typical set of seismic response behaviors belonging to *z=10* m. and *z=30* m. of the medium dense soil profile, respectively. Seismic response behaviors from these depths are selected so that typical behaviors from above and below $r^*_{u,f}$ boundary could be represented. In each figure, first, second and third column of subfigures belong to 2°, 10° and 15° slope angle cases. For *z=10* m. which is above $r^*_{u,f}$ curve, flow type of failure and large permanent displacements are expected for all slope angles analysed. Considering *z=30* m, medium dense profiles with 2°and 5°slope angles remain under $r^*_{u,f}$ boundary only, indicating no flow failure but permanent displacements.

Irrespective of depth, for lower slope angles, excess porewater pressure generation is higher and more gradual (Figure 10 a, b, c, and Figure 11 a, b, c). Accordingly, reduction in shear strength is higher as well (Figure 10 d, e, f, and Figure 11 d, e, f). At higher slope angles (10°, 15°), excess porewater pressure generation and therefore reduction in shear strength is lower, however, permanent lateral displacements are higher (Figure 10 j, k, l, and Figure 11 j, k, l). Higher value of permanent displacements are due to critical seismic acceleration coefficients, in $k^*_c(t)$ which for 10°, 15° cases decrease to zero very quickly during seismic excitation (Figure 10 g, h, i, and Figure 11 g, h, i). However, for slope angle of 2°, this decrease in $k^*_c(t)$ is more gradual.

Flow failure and the resulting deformations occur due to combined effect of shear strength reduction and gravity loading. With an increase in slope angle, gravity loading tends to govern behavior more than shear strength reduction and in this case, flow failure occurs at lower excess porewater pressure levels. During seismic excitation, once gravity loading due to initial static shear stress level catches up with the current shear strength level, excess porewater pressure can't find an opportunity to increase more and large flow deformations occur. On the other hand, with a decrease in slope angle (*slope angle β=2°, 5°*), increase in excess porewater pressures is more gradual and flow occurs more due to shear strength reduction than gravity loading.

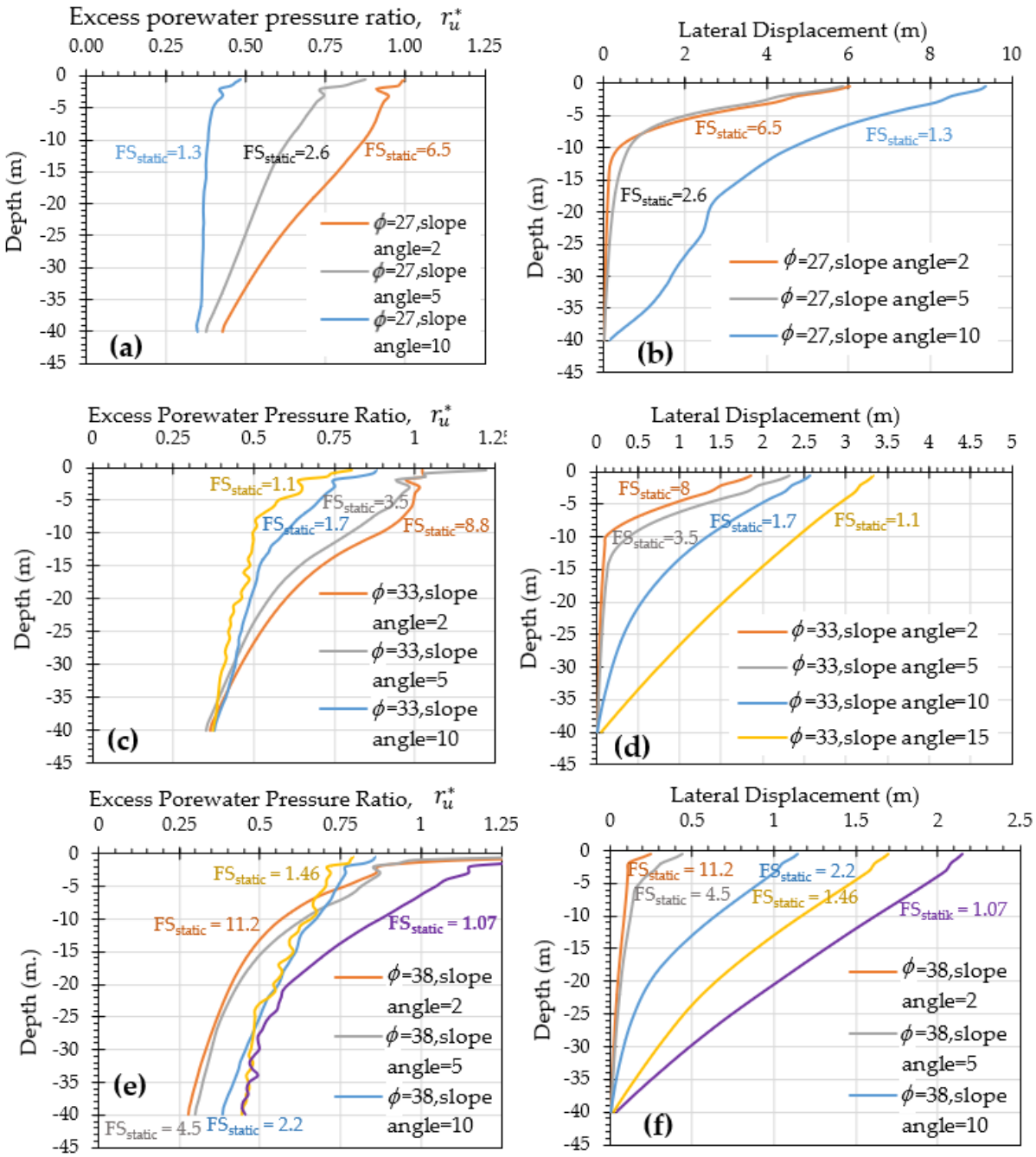

Figure 9. Variation of excess porewater pressure ratios and lateral displacements with respect to depth (a, b: loose state, c, d: medium dense state, e, f: dense state)

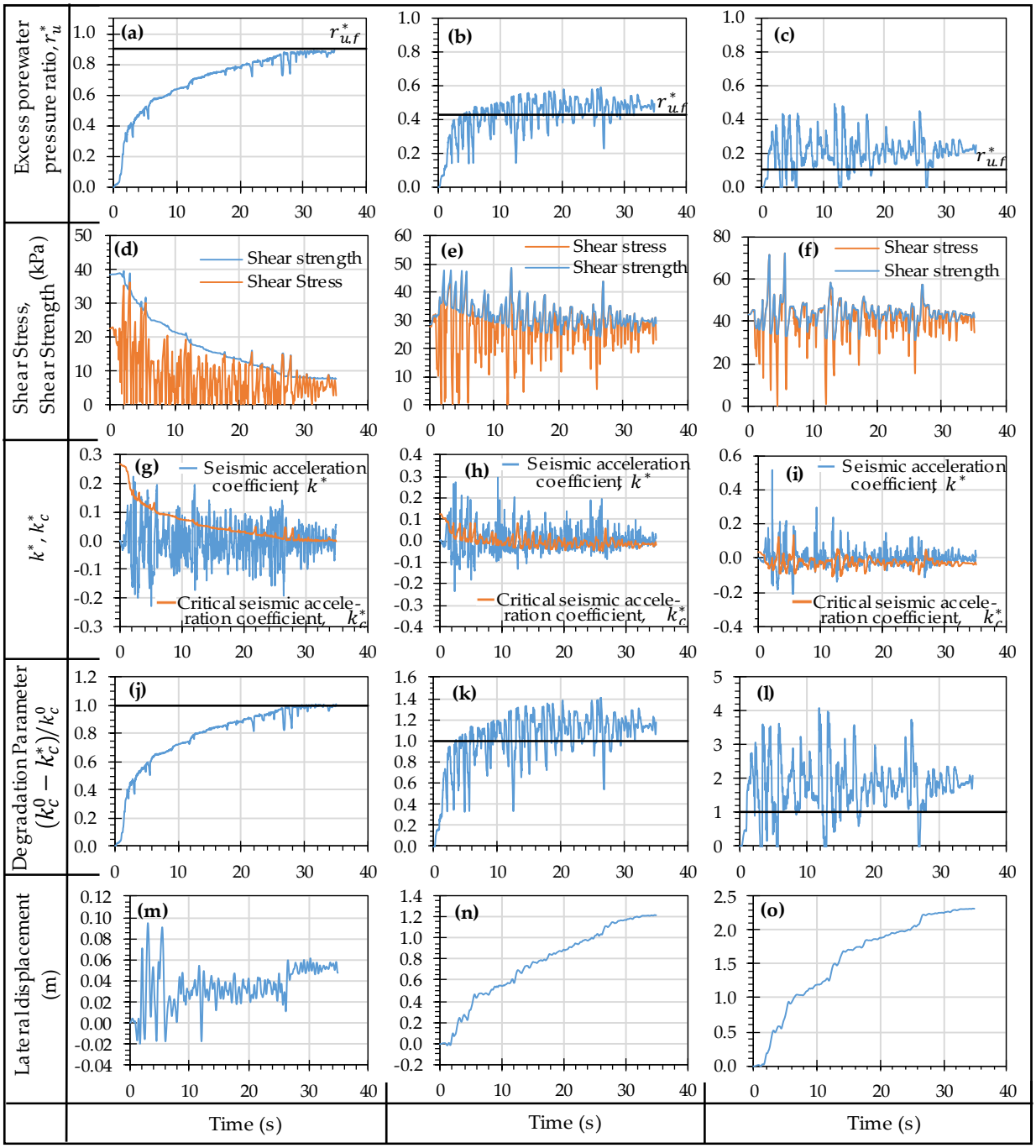

Figure 10. Effective stress based numerical analysis results at *z=10* m. of medium dense soil profile (Group of figures in the leftmost, middle and rightmost columns represent values for slope angles of 2°, 10°, 15° respectively).

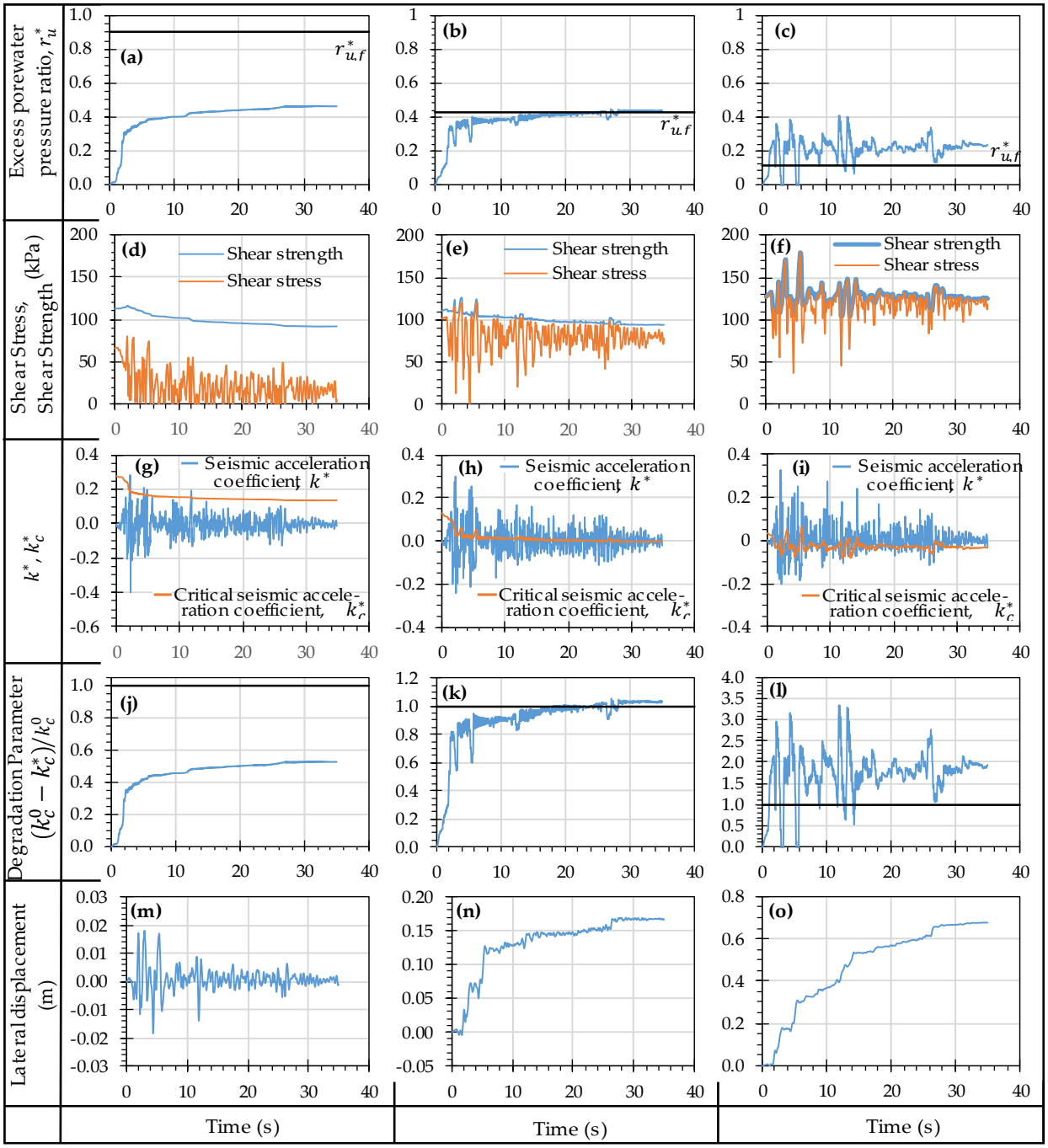

Figure 11. Effective stress based numerical analysis results at *z=30* m. of medium dense soil profile (Group of figures in the leftmost, middle and rightmost columns represent values for slope angles of 2°, 10°, 15° respectively).

Relationship Between Permanent Displacements and Degradation Parameter

Critical seismic acceleration coefficients degrade from an initial, non–degraded value (k_c^0) towards some minimum value of $k_{c,min}^*$ (degraded value corresponding to maximum excess porewater pressure, $r_{u,max}^*$) during seismic excitation (Figures 10 g, h, i, and Figure 11 g, h, i). Variation of k_c^0 with FS_{static} for each density state is presented in Figure 12 where it is clear that k_c^0 increases with density state of the soil profile. k_c^0 increases with FS_{static} up to some point and then stays constant thereof.

In case of lower slope angles, degradation of critical seismic acceleration coefficient is more gradual and goes in parallel with shear strength reduction due to excess porewater pressure generation. $k_c^* = 0$ case may occur when shear strength is fully lost, i.e liquefaction occurs. For higher slope angles, on the other hand, degradation of k_c^* is more sudden reaching a value of zero ($k_c^* = 0$) indicating the effect of shear strength reduction and gravity at the same time, however, gravity dominating more in most cases. Whatever the case is, if $k^* = a^*/g > k_c^*$, then permanent displacements are to be expected. Whenever shear strength reduction effects are in action, permanent displacements need to be evaluated based on the consideration of degradation effects on critical seismic acceleration coefficients. Most of the current correlations between critical seismic accelerations and permanent displacements are based on the non–degraded form of critical seismic accelerations, k_c^0 (Bray, J.D, 2007; Karray et al., 2018; Mendez et al., 2017;

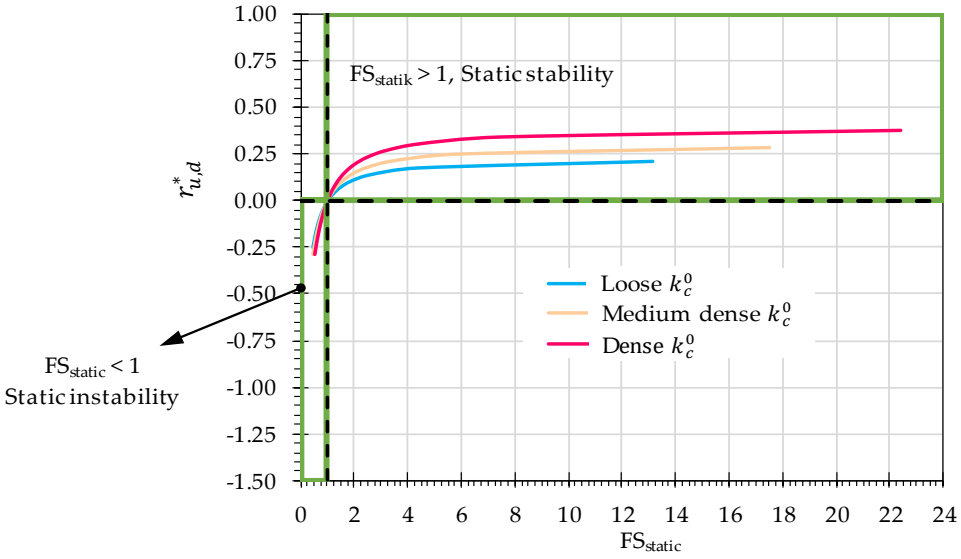

Figure 12. Variation of non-degraded critical seismic acceleration coefficient with FS_{static}.

Rampello et al., 2010; NCHRP, 2008). On the other hand, there is considerable amount of attempt to include degradation effect in the evaluation of permanent displacements (Biondi et al., 2007a, b; Ingegneri et al. 2019; Filippo and Cascone, 2019; Carlton and Kaynia, 2019; MAgistris, 2011; Cui et al., 2019; WSDOT Geotechnical Design Manual 2019). Figures 13, 14 and 15 exhibit variation of permanent lateral displacements along depth of each profile with the corresponding degradation parameter which is defined by $(Degradation\ parameter = (k_c^0 - k_c^*)/k_c^0)$. This parameter was proposed by Biondi et al. (2007a, b) for the consideration of shear strength effects in the evaluation of permanent

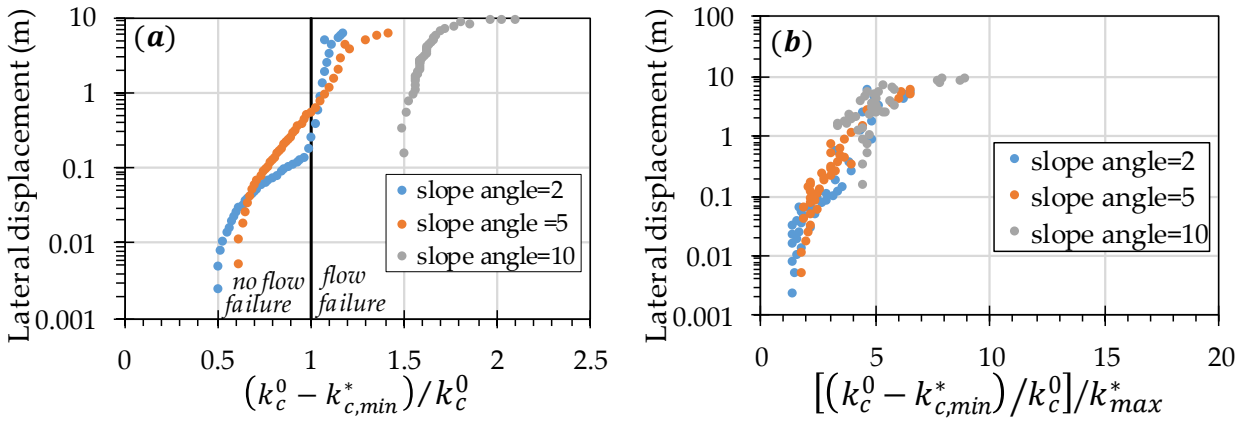

Figure 13. Variation of lateral permanent displacements with (a) degradation parameter (b) Degradation parameter $/k_{max}^*$ for the loose soil profile

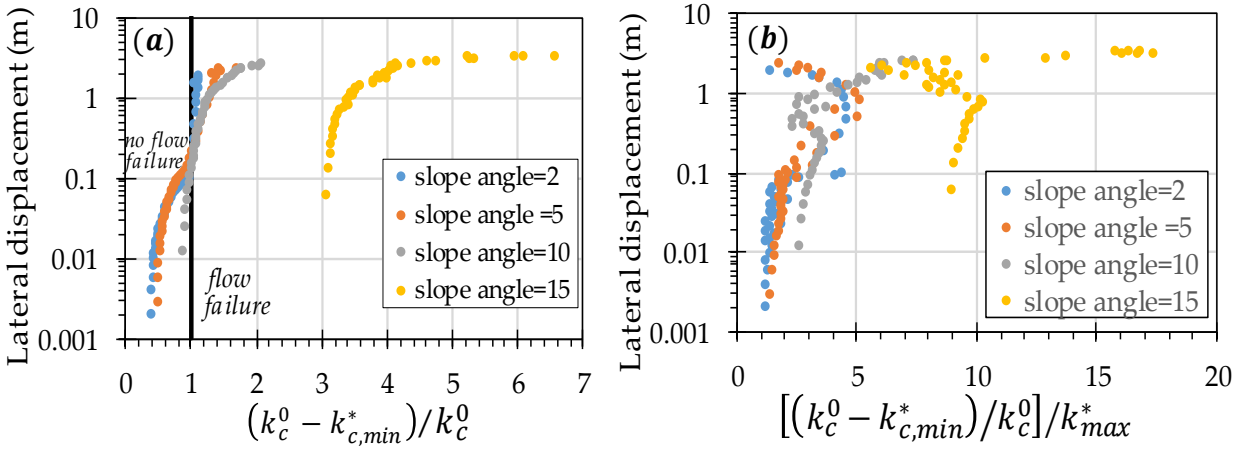

Figure 14. Variation of lateral permanent displacements with (a) degradation parameter (b) Degradation parameter $/k_{max}^*$ for the medium dense soil profile

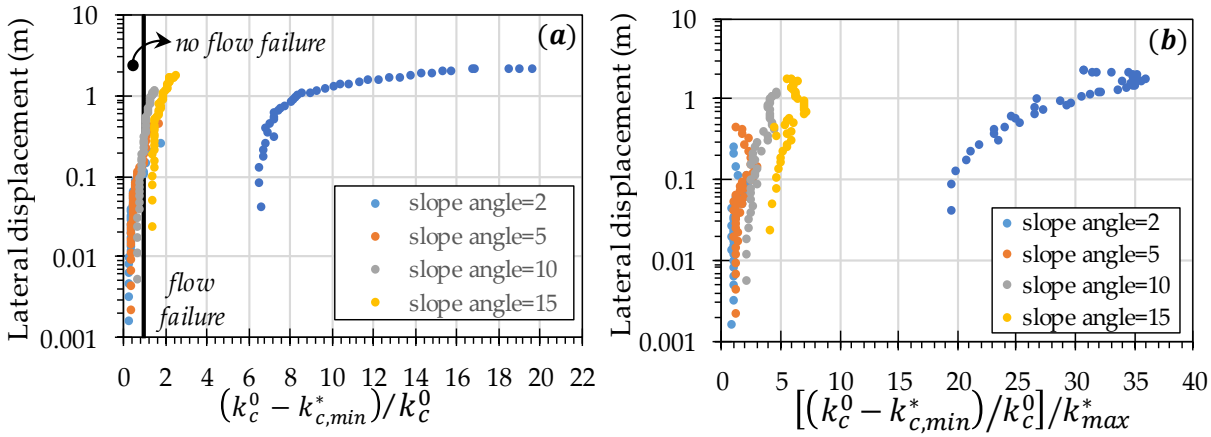

Figure 15. Variation of lateral permanent displacements with (a) degradation parameter (b) Degradation parameter $/k_{max}^*$ for the dense soil profile

displacements. Value of degradation parameter varies between 0–1. Permanent displacements corresponding to this range are not due to flow failure, however, those corresponding to degradation parameter >1 occur due to flow failure. Moreover, degradation parameter <0 indicates static instability of the slope as clearly seen in loose soil profile with 15° slope angle. It is clear from these figures that lateral permanent displacements > approximately 10 cm occur due to flow failure.

5. Conclusions

Slopes may loose their stability due to flow failures or due to excessive permanent deformations during earthquakes. Initial stress state defined through static factor of safety, inertial effects arising from seismic shear stresses and weakening effects arising from straining of the soil mass leading to excess porewater pressure generation and reduction in the available shear strength are the major factors governing seismic stability and permanent deformations.

In the context of this paper, 1-D effective stress based seismic response analysis have been conducted on loose, medium dense and dense saturated cohesionless infinite slopes with varying slope angles. Motivation behind such a work has been to inspect time dependent behavior of seismic shear stresses, excess porewater pressure generation, consequent shear strength variation and resulting accelarations and displacements. Understanding of how initial stress state (static stability state) and inertial + weakening effects govern seismic slope behavior is essential since it is the variation in the domination level of each mechanism which leads to various seismic response types of the same slope.

In addition, Biondi et al. (2002) and Biondi and Maugeri (2006) procedure (Modified

Newmark method for shear strength reduction effects) has been used for the evaluation of some threshold values concerning excess porewater pressure ratios and corresponding critical seismic acceleration coefficients. These thresholds indicate when flow failure is expected to be triggered and when permanent displacements (without flow failure) are expected to occur. Depending upon these threshold values, stability charts have been prepared for the analysed cases and whether flow failure or excessive permanent deformations are expected to occur along the soil profiles has been discussed. In addition, concept of degradation in critical seismic acceleration coefficients and its importance in the evaluation of permanent displacements have been highlighted.

References

Bandini, V., Biondi, G., Cascone, E., Rampello, S. (2015) A GLE-Based Model for Seismic Displacement Analysis of Slopes Including Strength Degradation and Geometry Rearrangement, Soil Dynamics and Earthquake Engineering, Vol. 71. Pp.128-142.

Biondi,G., Condorelli, A., Cascone, E., Mussumeci, G. (2004) Earthquake triggered landslide Hazards in the Catania Area, Management Information Systems, Vol.9, pp.115-130.

Biondi,G., Cascone, E., Maugeri, M. (2001) Seismic Response of Submerged Cohesionless Slopes, 4th. International Conference on Recent Advances in Geotechnical Earthquake Engineering and Soil Dynamics, March 26-31, Missouri University of Science and Technology.

Biondi G., Cascone,E., Maugeri,M., Motta,E. (2000) Pore Pressure Effect on Seismic Response of Slopes, 12th. World Conference on Earthquake Engineering, Auckland.

Biondi, G Cascone, E., Maugeri, M. (2002) Flow and Deformation Failure of Sandy Slopes, Soil Dynamics and Earthquake Engineering, Vol.22, pp.1103-1114

Biondi, G Cascone, E., Rampello, S. (2007a) Performance- Based Pseudo-Static Analysis of Slopes, 4ICEGE, 4th International Conference on Earthquake Geotechnical Engineering, Greece.

Biondi, G., Di Filippo, G., Maugeri, M. (2007b) Effect of Earthquake-Induced Porewater Pressure in Clay Slopes, 4ICEGE, 4th International Conference on Earthquake Geotechnical Engineering, Greece.

Biondi,G., Cascone, E., Maugeri, M. (2008) Evaluation of Pseudo-Static Coefficients according to Performance Based Criteria, Seismic Engineering Conference Commemorating the 1908 Messina and Reggio Calabria Earthquake (edt. by Santini Moraci), AIP, pp.501-508.

Biondi, G, Maugeri, M. (2006) A Modified Newmark Type Analysis According to EC-8 Requirements for Seismic Stability Analysis of Natural Slopes, ETC-12 Geotechnical Evaluation and Application of the Seismic Eurocode EC8 2003-2006, Ed. By Boucovolas, G., General Report, Proceedings of the Athens Workshop, pp.151-176.

Brabhaharan, P., Mason, D., Gkeli, E. (2018) Seismic Design and Performance of High Cut Slopes, NZ Transport Agency Research Report

613, Contracted Research Organisation – Opus International Consultants Ltd. P.149.

Bray, J.D (2007) Simplified Seismic Slope Displacement Procedures, Earthquake Geotechnical Engineering (Eds. K.D. Pitilakis), pp.327-353.

Carlton, B., Kaynia, A.M. (2019) Empirical Model for Seismically Induced Shear Strains in Slopes, Earthquake Geotechnical Engineering for Protection and Development of Environment and Constructions, Silvestri and Moraci (Eds.), Rome, Italy. Pp.1629-1637.

Cui, Y., Liu, A., Xu, C., Zheng, J. (2019) A Modified Newmark Method for Calculating Permanent Displacement of Seismic Slope Considering Dynamic Critical Acceleration, Advances in Civil Engineering, Vol.3., pp. 1-10.

Elgamal, A., Dobry, R., Parra, E., Yang, Z. (1998). Soil Dilation and Shear Deformations During Liquefaction. Proceedings of the 4th. International Conference On Case Histories in Geotechnical Engineering. Missauri University of Science and Technology.1238-1259.

Elgamal A., Yang, Z., Parra, E., Ragheb, A. (2003). Modelling of Cyclic Mobility in Saturated Cohesionless Soils. International Journal of Plasticity. 19, 883-905.

Elgamal, A. (2014). Site Liquefaction. Stress-Strain Response. Stress-Strain Models. Site Response. Lateral Deformation. Course Notes. Universidad Naciaonal de SanJuan, Argentina.

Filippo, G.D., Biondi, G., Cascone, E (2019) Influence of Earthquake-Induced Porewater Pressure on the Seismic Stability of Cohesive Slopes, Earthquake Geotechnical Engineering for the Protection and Development of Environment and Constructions, Eds. Francesco Silvestri and Nicola Moraci, Proceedings of the VII ICEGE 7th. International Conference On Earthquake Geotechnical Engineering, Rome, Italy, 17-20 June, 2019, pp. 2137-2144..

Ingegneri, S., Biondi, G., Cascone, E., Filippo, G.D. (2019) Influence of Cyclic Strength Degredation on a Newmark Type Analysis, Earthquake Geotechnical Engineering for the Protection and Development of Environment and Constructions, Eds. Francesco Silvestri and Nicola Moraci, Proceedings of the VII ICEGE 7th. International Conference On Earthquake Geotechnical Engineering, Rome, Italy, 17-20 June, 2019, p.2996-3004.

Jafarian, Y., Lashgari, A. (2017) Seismic Sliding Analysis of Sandy Slopes Subjected to Porewater Pressure Build Up, ASCE International Journal of Geomechanics, vol.17, Issue 11.

Jıa, J. (2018) Slope Stability Due to Seismic Loading (Chp. 8), Soil Dynamics and Foundation Modelling - Offshore and Earthquake Engineering, Springer, Aker solution, Bergen, Norway.

Karray, M., Hussien, M.,Delisle, M., Ledoux, C. (2018) Framework to Assess Pseudo-Static Approach for Seismic Stability of Clayey Slopes, Canadian Geotechnical Journal, Vol.55., No.12, pp.1-17.

Magistris, F.S. (2011) Beyond EC8: The New Italian Seismic Code, Geofizika, Vol.28. p.65-82.

Mendez, B., Taştan, E.O., Gutierrez, J. (2017) Performance Based Slope Stability Analysis

and the Pseudo-Static Factor of Safety, Geotechnical Frontiers 2017, Orlando, Florida, p.1-10.

NCHRP - Anderson D.G., Martin G.R, Lam I.P. and Wang JNJ, (2008), Seismic Analysis and Design of Retaining Walls, Buried Structures, Slopes and Embankments, Transportation Research Board, NCHRP - Report No. 611, p.148.

Parra, E. (1996). Numerical modeling of liquefaction and lateral ground deformation including cyclic mobility and dilation response in soil systems. Ph.D. thesis. Troy, N.Y.: Dept. of Civil Engineering, Rensselaer Polytechnic Institute.

Rampello, S., Callisto, L., Fargnoli, P. (2010) Evaluation of Slope Performance Under Earthquake Loading Conditions, Rivista Italiana Di Geotechnica, pp.29-41.

WSDOT (2019) Washington State Department of Transportation Geotechnical Design Manual. Chapter 6 Seismic Design, p. 80